A 7 GHZ ACOUSTICALLY COUPLED FILTER WITH INTRINSIC SWITCHABILITY USING FERROELECTRIC SCANDIUM-ALUMINUM NITRIDE

Sushant Rassay, Dicheng Mo, Roozbeh Tabrizian*
Department of Electrical and Computer Engineering, University of Florida, USA

ABSTRACT

This paper reports, for the first time, on an intrinsically switchable acoustically coupled filter at ~7 GHz, created using 200nm-thick ferroelectric scandium-aluminum nitride ($Sc_{0.28}Al_{0.72}N$) film. The filter operates based on coupling local thickness-extensional bulk acoustic wave (BAW) modes through zeroth-order symmetric (S_0) Lamb wave, in a monolithic structure with properly defined interdigitated transducers (IDTs). For the first time, intrinsic switchability of the acoustically coupled filter is achieved by depolarizing the transducer through application of low-frequency pulses and exploiting the ferroelectric behavior in $Sc_{0.28}Al_{0.72}N$. A filter prototype is presented with a center frequency of 6.9 GHz, -3dB bandwidth (BW) of 196 MHz (3% fractional BW), and a passband insertion-loss of ~6dB. The filter is switched between on and off states through application of 108V pulses at 25kHz between one of the IDT ports and the bottom electrode, resulting in on/off isolation exceeding 20dB. The high performance and intrinsic switchability along with the ultraminiaturized footprint of the presented super-high-frequency monolithic filter, highlights its potential for applications in configurable front-end module of the modern 5/6G wireless systems.

KEYWORDS

Ferroelectric, intrinsic switchability, scandium-aluminum nitride, acoustically coupled filter.

INTRODUCTION

With the exponential growth in wireless data traffic, due to the emergence of novel applications such as metaverse, IoT, and connected transportation, spectrum management becomes increasingly crucial. To accommodate the ever-increasing data rates, modern wireless technologies aim to use numerous new bands extended over ultra- and super-high-frequency regimes. Additionally, modern wireless systems increasingly rely on reconfigurable RF front-ends (RFFE) to enable low-latency communication and efficient use of spectrum resources.

Currently, spectral processing at the RFFE is performed by single-frequency / band electrically coupled bulk acoustic wave (BAW) filters that are arrayed through external switches. With the radical increase in communication bands, this architecture is not scalable considering the excessive increase in the number of filters and switches, and the resulting overhead on footprint and power consumption.

On the other hand, acoustically coupled filters provide several advantages over their electrically coupled counterparts that can alleviate the RFFE scaling to adopt new communication bands. These include reduction in the overall footprint of the filter, and lessening fabrication, routing and packaging complexities [1-3]. Acoustically coupled filters were introduced by Lakin, *et. al.*, in 2002 [4], and ever since have been widely explored as an alternative to electrically coupled filters.

This acoustic filter architecture operates based on effective coupling of two local thickness-extensional BAW resonance modes, excited under input and output IDTs, through guided Lamb waves. Benefiting from a single structure, While acoustically coupled filters provide significant reduction in footprint, and fabrication and integration complexity, they suffer from a higher insertion loss and lower bandwidth due to the partial electrode coverage inherent to the IDT design. However, these shortcomings can be relieved by using scandium-aluminum nitride films that provide substantially higher electromechanical coupling coefficient (k_t^2), compared to AlN. Additionally, the recent discovery of ferroelectricity in scandium-aluminum nitride [5] enables the use of polarization tuning for reconfiguration of acoustic resonators and filters [6-9].

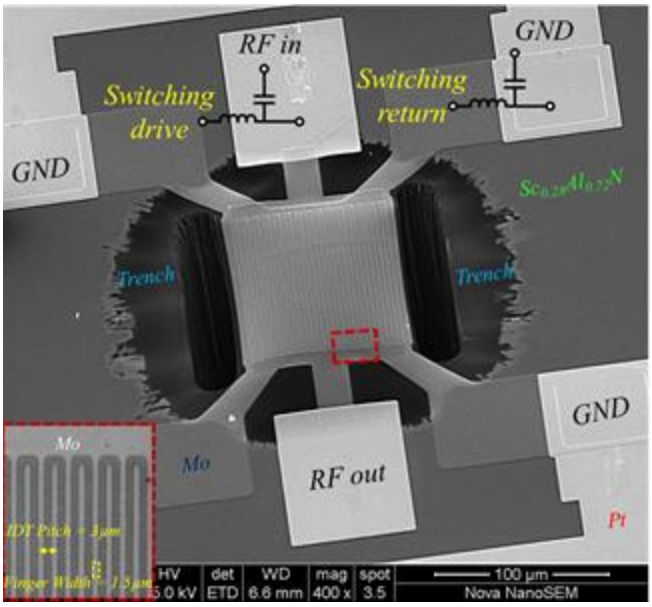

Fig. 1. The SEM image of the two-port intrinsically switchable acoustically coupled $Sc_{0.28}Al_{0.72}N$ filter. The RF and switching ports are identified. The inset shows the IDT dimensions.

In this work, we demonstrate the first intrinsically switchable acoustically coupled filter at 7 GHz, implemented in 200nm-thick $Sc_{0.28}Al_{0.72}N$ film. The intrinsic switchability is achieved through polarization tuning due to the ferroelectric behavior of $Sc_{0.28}Al_{0.72}N$. Figure 1 Shows the scanning electron microscope (SEM) image of the acoustically coupled filter, along with the RF and switching ports configuration.

OPERATION PRINCPLE

In this work, the acoustically coupled filter is realized by coupling the local thickness-extensional BAW under input and output IDTs through the S_0 Lamb wave. The BAW modes, which play a similar role to the shunt elements in ladder-type electrically coupled filters, are localized under IDT fingers due to the acoustic impedance mismatch with non-electroded regions. These local BAW modes are coupled together through the S_0 Lamb wave propagating across the non-electroded regions. With proper design of IDT pitch and electrode width, the Lamb wave propagation results in a second resonance mode with a frequency slightly higher than the anti-resonance of the local BAW modes. This Lamb mode plays a similar role to the series element in ladder-type electrically coupled filters. This operation concept is schematically shown in fig. 2, where the BAW and Lamb modes are represented by RLC

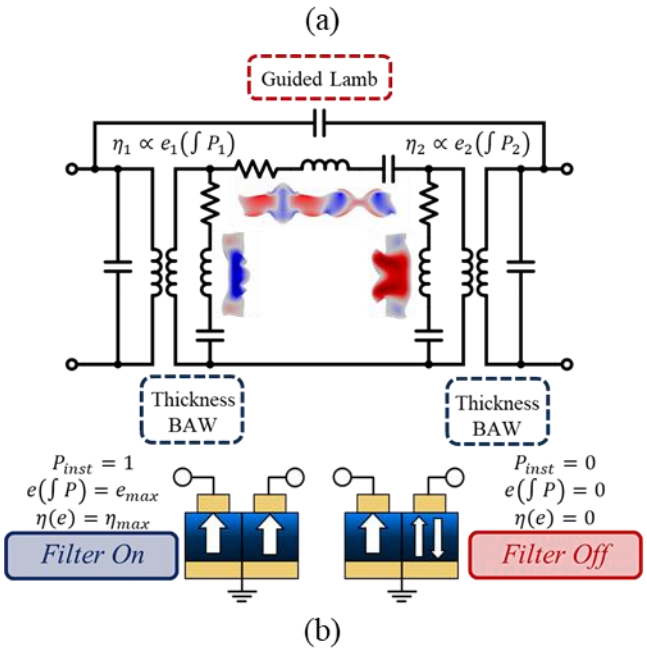

Fig. 2. (a) Electromechanical equivalent model of the acoustically coupled filter and the constituent resonance modes. (b) Conceptual intrinsic switching principle showing the filter in On and off states. These states are defined by the net polarization under the IDT ports.

branches placed in shunt and series, respectively. The COMSOL simulated deformation mode-shape for each element is also shown.

The electromechanical transduction of the filter is represented by two transformers at the input and output ports, along with the corresponding static capacitors. The transformer ratios are identified by the IDT finger width and are proportional to the piezoelectric coefficients (e_{ij}) of the film. Considering the ferroelectricity in $Sc_{0.28}Al_{0.72}N$, e_{ij} can be tuned by polarization switching through application of low-frequency pulses with amplitude close to the coercive field [9]. Depending on the magnitude and number of applied switching pulses, a finite number of ferroelectric domains (*i.e.*, single-crystal grains within the polycrystalline $Sc_{0.28}Al_{0.72}N$ film) reverse their polarity. This results in cancelation of electromechanical transduction and reduces effective e_{ij} in pulsed region of the film. In an ideal case, when the polarization in half of ferroelectric domains is reversed, the effective e_{ij} is nulled and electromechanical transduction is switched off.

The intrinsic switching principle is represented in equivalent model of the filter (fig. 2) by polarization-dependent transduction efficiency of transformers. Upon application of sufficient pulses between one or both of IDTs and the bottom electrode through a bias-tee, the net polarization (*i.e.*, $\int P$) under one or both IDT ports is nulled, and the filter is switched off. Continuing application of switching pulses, to fully reverse the polarization of the entire domains, switches the filter back to the on state.

FABRICATION PROCESS

The fabrication process flow for realization of the $Sc_{0.28}Al_{0.72}N$ acoustically coupled filters is shown in fig. 3. The process consists of DC sputtering deposition of 100nm Mo layer, atop a 30nm AlN film that serves as the seed for (110)-textured growth of Mo. Bottom Mo layer is then patterned using a boron trichloride (BCl_3) based recipe in a reactive-ion-etching inductively coupled plasma (RIE-ICP) system. To ensure crack-free growth of the subsequent films, the Mo film is patterned using tapered photoresist masks created

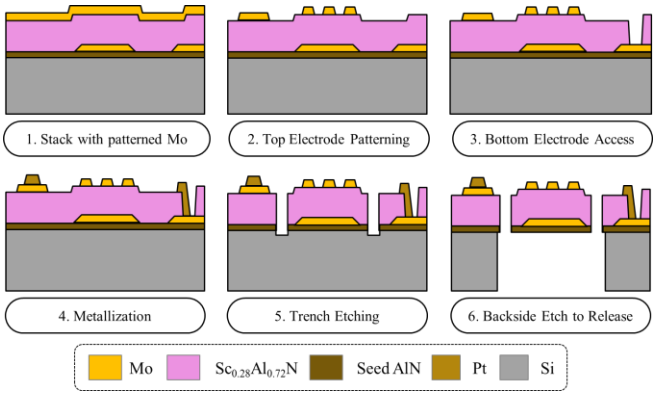

Fig. 3. Fabrication process flow for implementation of acoustically coupled filter in a 200nm-thick $Sc_{0.28}Al_{0.72}N$ films, based on using a six-mask process for patterning electrodes and releasing structure.

by proximity exposure method. The resulting tapered sidewalls of the bottom Mo patterns enables crack-free growth of the $Sc_{0.28}Al_{0.72}N$ layer.

Following bottom electrode patterning, a c-axis textured 200nm-thick $Sc_{0.28}Al_{0.72}N$ layer is deposited using reactive magnetron sputtering from segmented scandium-aluminum targets [10, 11]. Next, a 150nm thick Mo layer is DC sputtered and patterned using SF_6 in RIE-ICP, to create top IDT ports of the filter.

This is followed by etching $Sc_{0.28}Al_{0.72}N$, using a Cl_2-based recipe in RIE-ICP, to access bottom Mo. Next, a 500nm-thick platinum (Pt) is lifted-off to create the pads. Lateral geometry of the resonator is then formed by etching trenches using a high power Cl_2/BCl_3 based recipe in the RIE-ICP system and PECVD SiO_2 as the hard-mask. Finally, the device is released from the backside of the Si substrate by deep reactive ion etching (DRIE).

CHARACTERIZATION

The RF performance of the fabricated filters are characterized using Keysight 5222A Vector Network Analyzer (VNA), along with a short-open-load-through (SOLT) calibration procedure enabled by CS-5 calibration kit. Ferroelectric hysteresis characterization and filter switching is performed using a Radiant PiezoMEMS ferroelectric tester.

The measured filter transmission and reflection responses (*i.e.*, $|S_{21}|$ and $|S_{11}|$) are shown in fig. 4. A center frequency of 6.9 GHz, a

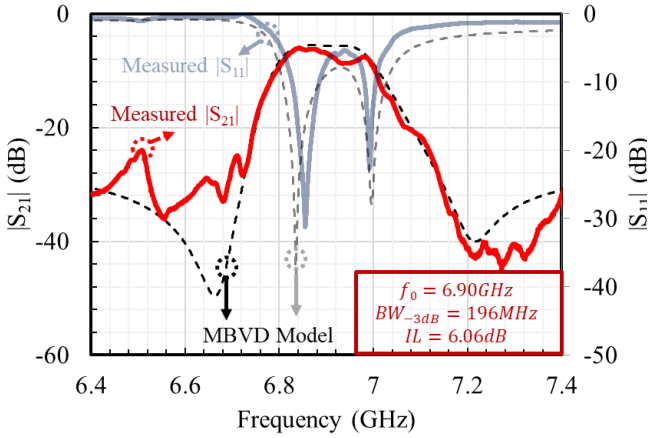

Fig. 4. The measured $|S_{21}|$ and $|S_{11}|$ responses of the filter with a BW_{-3dB} of ~196MHz at 6.9GHz. The measured response is compared to the response obtained from the MBVD model shown in fig. 5.

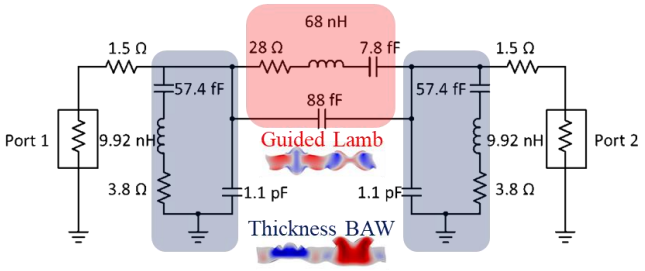

Fig. 5. The electrical equivalent circuit of the acoutically coupled filter. The deformation shape of consitutent BAW and Lamb modes are also shown by the corresponding resonator element.

BW_{-3dB} of 196 MHz (~3% fractional bandwidth), and an insertion loss (IL) of 6.06dB is extracted.

Figure 4 also shows the fitted response from the MBVD model of the filter, with electrical equivalent circuit detailed in fig. 5. An accurate match of the measured and modeled responses is evident, confirming the discussed operation principle of the acoustically coupled filter.

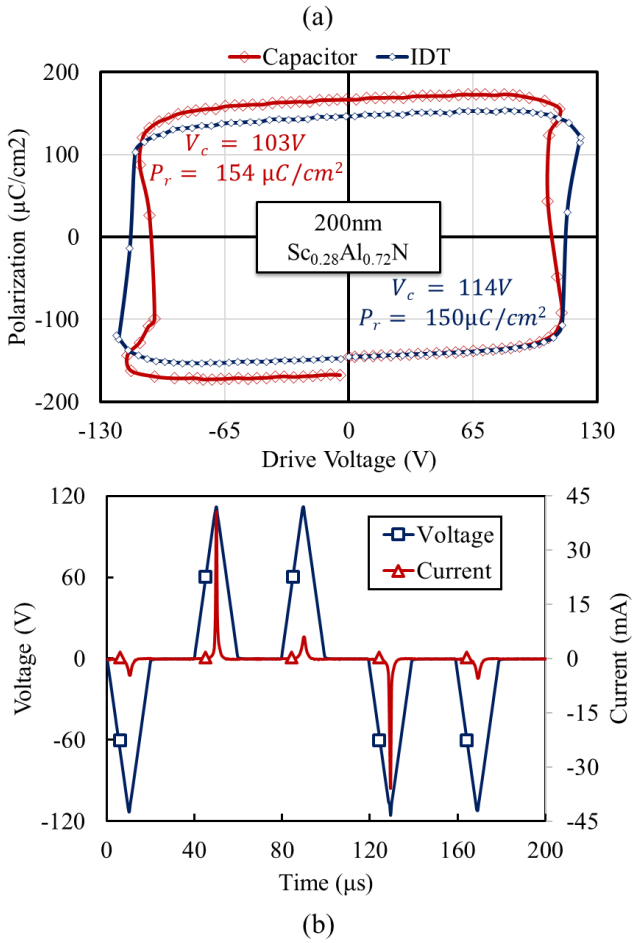

Fig. 6. (a) Comparison of the measured polarization-voltage hysteresis loops at one of the IDT ports (prior to resonator release) and a 100μm×100μm capacitor. (b) Measured instantaneous current for the PUND test to determine accurate voltage needed for switching filter between on and off states.

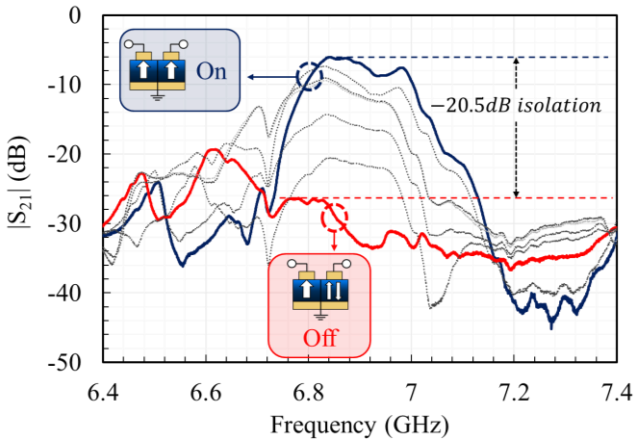

Fig. 7. Measured transmission response of the acoustically coupled filter and its evolution upon application of single triangular pulses at -108V leading to depolarized (i.e., off) state after the fifth pulse.

To identify the required switching voltage, the polarization hysteresis of ferroelectric $Sc_{0.28}Al_{0.72}N$ film is measured. Figure 6 (a) shows the polarization hysteresis loop under the IDTs in comparison with a 100μm×100μm capacitor. The polarization loops are measured by applying bipolar triangular pulses at 100kHz frequency and with 125V amplitude. A 114V coercive voltage is extracted from the loop for IDT capacitor, which identifies the switching voltage of the filter. Figure 6 (b) shows the instantaneous current measured upon driving the IDT capacitor with a 45kHz negative positive-up-negative-down (PUND) pulse sequence. The significant change in instantaneous current when the sign of driving voltage pulse is changed corresponds to the $Sc_{0.28}Al_{0.72}N$ film polarization transitioning between metal- and nitrogen-polar states.

A pulse amplitude of 108V, which is slightly smaller than the coercive voltage, is used for filter switching. This enables access to depolarization state with nulled electromechanical transduction (*i.e.*, the filter Off state) with application of 5 pulses. Pulsed switching is performed using 25kHz triangular monopolar train with a voltage of 108V, to depolarize / polarize resonator for Off/On operation.

Figure 7 shows the filter transmission response evolution from the On-state to Off-state (*i.e.*, depolarized transducer) by application of monopolar triangular pulses to one of the resonator ports. The resonator turns completely off after application of 5 pulses, resulting in a ~20.5dB isolation. While application of negative monopolar pulses on one of IDT ports results in the gradual increase of the IL in filter passband, it may induce undesirable excitation of spurious modes, as evident in fig. 7. These modes can be further suppressed by application of the switching depolarization pulses to the second IDT port. This will be further explored in future publications.

CONCLUSION

This paper, for the first time, demonstrates an intrinsically switchable acoustically coupled filter created in $Sc_{0.28}Al_{0.72}N$, with a center frequency of ~6.9 GHz and a BW_{-3dB} of 196 MHz. Intrinsic switchability is achieved through application of consecutive triangular monopolar pulses of 108V to one of IDT ports of the filter, resulting in polarization and depolarization of the piezoelectric transduction to switch the filter between On and Off states, respectively. The filter operation principle, based on coupling thickness-extensional BAW modes with S_0 Lamb waves, concept is presented, and the switching principle based on ferroelectric polarization tuning in $Sc_{0.28}Al_{0.72}N$ is discussed. The filter prototype is switched between On and Off states through application of 25kHz

pulses at 108V to one of the filter ports. An on/off isolation of ~20.5dB is achieved. The high performance and intrinsic switchability of the presented $Sc_{0.28}Al_{0.72}N$ acoustically coupled filter highlight its potential for application in configurable super-high-frequency RF front-end of emerging 5G/6G systems.

ACKNOWLEDGEMENT

The authors would like to thank the staff at Nanoscale Research Facility at the University of Florida with device fabrication support. This work was supported in parts by the Defense Advanced Research Projects Agency (DARPA), Tunable Ferroelectric Nitrides (TUFEN) Program under Grant HR00112090049, and the National Science Foundation (NSF) through the CAREER award (Grant ECCS-1752206).

REFERENCES

[1] R. Abdolvand and F. Ayazi, "Monolithic Thin-Film Piezoelectric-on-Substrate Filters," 2007 IEEE/MTT-S International Microwave Symposium, 2007, pp. 509-512, doi: 10.1109/MWSYM.2007.380519.

[2] T. Pensala, T. Makkonen, J. Dekker and M. Ylilammi, "Laterally Acoustically Coupled BAW Filters at 3.6 GHz," 2018 IEEE International Ultrasonics Symposium (IUS), 2018, pp. 1-4, doi: 10.1109/ULTSYM.2018.8579900.

[3] W. Pan, V. A. Thakar, M. Rais-Zadeh and F. Ayazi, "Acoustically coupled thickness-mode AIN-on-Si band-pass filters-part I: principle and devices," in IEEE Transactions on Ultrasonics, Ferroelectrics, and Frequency Control, vol. 59, no. 10, pp. 2262-2269, October 2012, doi: 10.1109/TUFFC.2012.2451.

[4] K. M. Lakin, "Coupled resonator filters," 2002 IEEE Ultrasonics Symposium, 2002. Proceedings., 2002, pp. 901-908 vol.1, doi: 10.1109/ULTSYM.2002.1193543.

[5] S. Fichtner, N. Wolff, F. Lofink, L. Kienle, & B. Wagner, "AlScN: A III-V semiconductor based ferroelectric," Journal of Applied Physics, 125(11), 114103 (2019).

[6] S. Rassay, F. Hakim, M. Ramezani and R. Tabrizian, "Acoustically Coupled Wideband RF Filters with Bandwidth Reconfigurablity Using Ferroelectric Aluminum Scandium Nitride Film," 2020 IEEE 33rd International Conference on Micro Electro Mechanical Systems (MEMS), 2020, pp. 1254-1257, doi: 10.1109/MEMS46641.2020.9056353.

[7] S. Rassay, D. Mo, C. Li, N. Choudhary, C. Forgey and R. Tabrizian, "Intrinsically Switchable Ferroelectric Scandium Aluminum Nitride Lamb-Mode Resonators," in IEEE Electron Device Letters, vol. 42, no. 7, pp. 1065-1068, July 2021, doi: 10.1109/LED.2021.3078444.

[8] S. Dabas, D. Mo, S. Rassay and R. Tabrizian, "Intrinsically Tunable Laminated Ferroelectric Scandium Aluminum Nitride Extensional Resonator Based on Local Polarization Switching," 2022 IEEE 35th International Conference on Micro Electro Mechanical Systems Conference (MEMS), 2022, pp. 1050-1053, doi: 10.1109/MEMS51670.2022.9699790.

[9] D. Mo, S. Rassay and R. Tabrizian, "Intrinsically Switchable Ferroelectric Scandium Aluminum Nitride Bulk Acoustic Wave Resonators," 2021 21st International Conference on Solid-State Sensors, Actuators and Microsystems (Transducers), 2021, pp. 317-320, doi: 10.1109/Transducers50396.2021.9495634.

[10] V. Felmetsger, M. Mikhov, M. Ramezani and R. Tabrizian, "Sputter Process Optimization for Al0.7Sc0.3N Piezoelectric Films," 2019 IEEE International Ultrasonics Symposium (IUS), 2019, pp. 2600-2603, doi: 10.1109/ULTSYM.2019.8925576.

[11] S. Rassay, F. Hakim, C. Li, C. Forgey, N. Choudhary, & R. Tabrizian, "A Segmented-Target Sputtering Process for Growth of Sub-50 nm Ferroelectric Scandium–Aluminum–Nitride Films with Composition and Stress Tuning", physica status solidi (RRL)–Rapid Research Letters, 15(5), 2100087, (2021).

CONTACT

*Sushant Rassay, tel: +1-321-616-1298; sushantrassay@ufl.edu.